Brain Topography, Volume 19, Numbers 1/2, Winter 2006 (© 2006)
DOI: 10.1007/s10548-006-0011-0

Spherical Splines and Average Referencing in Scalp Electroencephalography

Thomas C. Ferree

Summary: EEG analysis and interpretation are affected by the reference electrode. Average referenced potentials are used widely to approximate the potentials relative to infinity, but estimates of the average surface potential are prone to errors due to incomplete sampling of the scalp surface. Even if the electrode density is high, this arises by not sampling the inferior scalp surface. This paper shows analytically how the spherical splines represent the average surface potential. It also shows that, for spline orders $m \geq 3$, the interpolating function is well approximated by its large-m limit, weighting near and distant electrodes with opposite signs. Together these motivate the hypothesis that spherical splines permit a better estimate of the potentials relative to infinity than the discrete average computed over superior scalp electrodes. It tests this hypothesis using numerical simulations in a four-sphere head model with single- and many-dipole sources, and variations in spline order, electrode number and head model parameters. The results confirm that the spherical splines yield a better estimate of the potentials relative to infinity, provided the electrode sampling density is adequate.

Key words: EEG; Reference; Interpolation; Topographic map; Skull conductivity.

1. Introduction

Modern EEG systems use many (64-256) scalp electrodes, each measuring the voltage at its location relative to some reference location. The nature of voltage measurements and noise considerations require the reference electrode be placed on the scalp, where it is not quiet but is sensitive to brain activity (Nunez et al. 1981). Ways of avoiding this problem include referencing to the average scalp potential, analyzing bipolar pairs for which the reference effect is explicit, and computing the scalp surface Laplacian using local or global splines. In theory the average referenced potential has two favorable properties: it is independent of any particular choice of reference electrode, and it approximates at each point the potential relative to infinity (Bertrand et al. 1985). Because it can not be determined precisely, the average reference has received valid criticism (Tomberg et al. 1990; Desmedt and Tomberg 1990) in favor of explicit references (Gencer et al. 1996; Geselowitz 1998), the surface Laplacian (Hjorth 1975; Nunez 1981), or more complicated methods (Lehmann et al. 1986; Yao 2001; Orekhova et al. 2002).

Two approaches to spline interpolation are common in EEG. Thin-plate splines (Duchon 1976; Perrin et al. 1987) are more general, allowing data interpolation on arbitrary-shaped surfaces. Spherical splines, first introduced to EEG by Perrin et al. (1989, 1990), are more common because they are easier to implement and seem consistent with the widely used spherical head models. The splines were derived via a mechanical analogy, wherein a thin material plate was deformed to minimize the fitting error and the mechanical energy associated with bending of the plate (Wahba and Wendelberger 1980; Wahba 1981, 1982). The derivation does not involve the physics of electric fields in the head. Thus application of the spherical splines to EEG data is justified only by numerical simulations of dipole sources in the brain. Several studies have compared spline interpolation methods and orders in EEG (Soong et al. 1993; Fletcher et al. 1996), and found overall agreement with some differences.

For real EEG data, splines are fit to the potential at the electrodes, which imperfectly sample the superior surface of the head, and completely neglect the inferior head surface. Of course, the outer head surface is not topologically closed at the neck. Still this incomplete sampling introduces a bias into the estimation of the average reference, and has been termed the polar average reference effect (Junghofer et al. 1999). These authors noted that spherical splines improve the estimation of the average reference potential, but provided no theoretical basis and did not elaborate their performance.

Simple considerations show that the spherical splines represent the average surface potential

Accepted for publication: August 12, 2006; Published Online: October 4 2006.

Correspondence and reprint requests should be addressed to Thomas C. Ferree, Center for Mind and Brain, University of California, Davis, CA 95616. E-mail: tom.ferree@gmail.com

transparently, and weight each electrode spatially in a way that is qualitatively consistent with dipole fields. Together these observations motivate the hypothesis that spherical splines should provide a better estimate of the average scalp potential than the discrete average computed over superior scalp electrodes. This paper develops these ideas, and tests the stated hypothesis using a four-sphere head model with a variety of dipole source configurations and electrode arrays.

2. Methods

2.1. Spherical Splines

Let $\vec{r}_j$ denote the location of a measurement electrode on the spherical scalp surface, $j = 1, \ldots, N$. Let $\vec{r}$ denote the location of an arbitrary surface point, and let $V(\vec{r})$ denote the potential at that point (relative to some reference point). Spherical splines estimate the potential $V(\vec{r})$ by

$$V(\vec{r}) = c_0 + \sum_{j=1}^{N} c_j \, g_m(\hat{r} \cdot \hat{r}_j) \tag{1}$$

where c_0 and c_j are constants fit to the data. The dot product $\hat{r} \cdot \hat{r}_j$ is the cosine of the angle between the interpolation point $\vec{r}$ and electrode location $\vec{r}_j$. The function $g_m(x)$ is given by

$$g_m(x) = \frac{1}{4\pi} \sum_{n=1}^{\infty} \frac{2n+1}{(n(n+1))^m} P_n(x) \tag{2}$$

where the $P_n(x)$ are the ordinary Legendre polynomials.

2.2. Fitting the Spline Coefficients

The $N+1$ coefficients c_j in (1) are determined by imposing two conditions (Wahba 1981, 1982). First, the interpolation function must reproduce the data when evaluated at the electrodes:

$$V(\vec{r}_i) = c_0 + \sum_{j=1}^{N} c_j \, g_m(\hat{r}_i \cdot \hat{r}_j) \tag{3}$$

for $i = 1, \ldots, N$. Second, the coefficients c_j must sum to zero:

$$\sum_{j=1}^{N} c_j = 0 \tag{4}$$

Together these conditions constitute $N+1$ equations for the $N+1$ coefficients c_0 and c_j.

These equations were concatenated to form a single set of $N+1$ equations, and solved by singular value decomposition and back substitution (Press et al. 1992). Perrin et al. (1989) mentioned a regularization method. For the electrode arrays used here, which are not geometrically perfect but were measured on real subjects, the matrix for the $N+1$ system was full rank and did not require regularization.

2.3. Average Reference Potential

Let $\Phi(\vec{r})$ denote the scalp potential at point $\vec{r}$ due to dipole sources in the head. This potential is measured relative to infinity, i.e., the *absolute* scalp potential. Let V_i denote the scalp potentials measured at electrodes $i = 1, \ldots, N$. The last electrode $i = N$ is the reference electrode for which $V_N \equiv 0$. For a perfect EEG amplifier system, we have $V_i = \Phi_i - \Phi_{\text{ref}}$, where $\Phi_i = \Phi(\vec{r}_i)$, and $\Phi_N = \Phi_{\text{ref}}$ is the absolute potential at the reference electrode. We seek Φ_i but measure V_i; the difference amounts to estimating Φ_{ref}.

Let $\bar{V}$ denote the average of the potentials measured at N scalp electrodes:

$$\bar{V} \equiv \frac{1}{N} \sum_{i=1}^{N} V_i \tag{5}$$

Let U_i denote the average referenced potentials, i.e., rereferenced according to the definition $U_i \equiv V_i - \bar{V}$. The U_i have the property

$$\frac{1}{N} \sum_{i=1}^{N} U_i = \frac{1}{N} \sum_{i=1}^{N} \left(V_i - \bar{V}\right) = \left(\bar{V} - \bar{V}\right) = 0 \tag{6}$$

Because the sum over the U_i vanishes like the surface integral of Φ, the U_i are taken to estimate the Φ_i, with $\Phi_{\text{ref}} \equiv \Phi_N \simeq U_N = -\bar{V}$. This estimate is biased by not including contributions from the inferior head surface: the polar average reference effect (Junghofer et al. 1999).

Despite their long and widespread use in scalp EEG, it has not yet been articulated how the spherical splines represent the average potential in the constant c_0. The present paper begins with this observation, and the goal of estimating more accurately the reference potential Φ_{ref}. Integrating (1) over the entire spherical scalp surface, and using that the integral of $P_n(x)$ on $-1 \le x \le +1$ vanishes for $n \neq 0$ (Arfken 1995), leads to

$$c_0 = \frac{1}{4\pi r_4^2} \int V(\vec{r}) \, dS \tag{7}$$

where r_4 is the outer scalp radius. Thus the coefficient c_0 is equal to the average of the interpolated potential over the sphere surface. Provided the spline fit is internally consistent, this relation should hold true exactly (to within numerical precision). The remaining question is how well $V(\vec{r})$ matches the actual potential, particularly on the inferior head surface.

Current conservation implies that, for dipolar current sources in an arbitrary volume conductor, the surface integral of the absolute potential Φ vanishes (Bertrand et al. 1985). Substituting $V(\vec{r}) = \Phi(\vec{r}) - \Phi_{\text{ref}}$ leads to

$$c_0 = \frac{1}{4\pi r_4^2} \int (\Phi(\vec{r}) - \Phi_{\text{ref}})\ dS \simeq -\Phi_{\text{ref}} \qquad (8)$$

Based upon (8), we expect c_0 to provide a *reasonable* estimate of Φ_{ref}, which can be used to compute the absolute potentials using $\Phi_i = V_i + \Phi_{\text{ref}} \simeq V_i - c_0$.

Of course, this favorable situation is limited by the fact that the spline fit is severely under-constrained on the inferior head surface, and is unlikely to be numerically accurate there. It is conceivable that the estimate $\Phi_{\text{ref}} \simeq -c_0$ is *worse* than the usual estimate $\Phi_{\text{ref}} \simeq -\bar{V}$, but further investigation shows that is not the case. An argument that spherical splines should provide a *better* estimate of Φ_{ref} is given next.

2.4. Limiting Behavior for Large m

When applied to scalp EEG, the spherical splines perform best when the spline order $m = 3$ or 4 (Perrin et al. 1989; Soufflet et al. 1991), and these values have been adopted in most studies. Visual inspection of (2) suggests that the sum converges rapidly as a function of m. For some m, the $n = 1$ term dominates and the seemingly complicated expression (2) reduces to

$$g_m(x) \simeq \frac{1}{4\pi} \frac{3}{2^m}\ x \equiv a_m\ x \qquad (9)$$

because $P_1(x) = x$. In this limit the function $g_m(\hat{r} \cdot \hat{r}_j)$ in (1) is simply proportional to $\hat{r} \cdot \hat{r}_j$, the cosine of the angle between the interpolation point $\vec{r}$ and the measurement point $\vec{r}_j$. This observation aids intuition on the spherical splines, and supports the following argument.

2.5. Hypothesis

Consider a dipole located centrally and oriented upward. For a certain sign convention, the potential on the scalp is positive for $0 \leq \theta < 90$, and negative for $90 < \theta \leq 180$. An electrode array which covers only the upper scalp surface ($\theta \leq 135$) will bias $\bar{V}$ toward positive values. The potential on the inferior scalp surface estimated with spherical splines will weight the superior potentials with a value near $-a_m$, causing the inferior potential to be negative. Of course, the potential estimated on the inferior surface will not be accurate when only superior electrodes are used to fit the splines. Nevertheless, the spline-based estimate of the inferior surface potential will have the correct sign, and bias c_0 in the correct direction. In this way, the spline function $g_m(x)$ is qualitatively consistent with dipole fields for the purpose of extrapolating to the inferior scalp surface.

Based upon this observation, it is hypothesized that the spherical spline coefficient c_0 should generally provide a *better* estimate of Φ_{ref} than the usual estimate $\bar{V}$. Since (1) is linear in the potential data, the simple example above is expected to generalize to arbitrary configurations of brain dipoles. This hypothesis is tested numerically for spline orders $m = 3$ and 4, electrode numbers $N = 19, 65, 129$, and variations in the head model parameters and dipole source configurations.

2.6. Four-Sphere Head Model

Scalp potentials were simulated by placing dipoles in a four-sphere head model. The head radii were set to standard values: $r_1 = 8.0$ (brain), $r_2 = 8.2$ (inner skull), $r_3 = 8.7$ (outer skull), and $r_4 = 9.2$ cm (scalp). The spherical scalp was fitted with a 19-electrode clinical array, and 65- and 129-electrode arrays (Electrical Geodesics, Inc., Eugene, Oregon) with reference electrode located at the vertex. Each array samples the superior scalp surface slightly differently. The distributions of electrode angles θ_i from the positive z-axis (near the vertex) have the following statistics: for $N = 19$, $\theta_{\text{mean}} = 72^\circ$, $\theta_{\text{max}} = 96^\circ$; for $N = 65$, $\theta_{\text{mean}} = 84^\circ$, $\theta_{\text{max}} = 140^\circ$; for $N = 129$, $\theta_{\text{mean}} = 62^\circ$, $\theta_{\text{max}} = 123^\circ$. Note that the 65-electrode array, not the 129-electrode array, extends furthest over the inferior head surface.

Aside from inhomogeneities and anisotropies ignored in spherical head models, the conductivity of head tissues are known within some (perhaps large) range of error (Foster and Schwan 1989). The brain conductivity $\sigma_1 \simeq 0.15\,\text{S/m}$ (Stoy et al. 1982). The CSF conductivity $\sigma_2 \simeq 1.79\,\text{S/m}$ (Baumann et al. 1997). The scalp conductivity $\sigma_4 \simeq 0.44\,\text{S/m}$ (Geddes and Baker 1967). The conductivity of the living human skull, however, has been a source of continued debate. Rush and Blanchard (1966) measured the conductivity ratio between the skull and saline in which the skull was immersed, and found conductivity ratios ranging from 50 to 300. Rush and Driscoll (1968) found a ratio near 80, then applied that ratio between the brain and skull, as though the living skull were saturated with brain-like rather than saline-like fluid. Most subsequent studies (e.g., Stok 1987) have used this ratio. Assuming the brain conductivity $\sigma_1 \simeq 0.15\,\text{S/m}$, for example, $\sigma_1/\sigma_3 \simeq 80$ implies $\sigma_3 \simeq 0.002\,\text{S/m}$. Since then evidence has accumulated that this early measurement may greatly underestimate σ_3. Even within the context of the Rush and Driscoll (1968) study, assuming the saline conductivity $\sigma \simeq 1.3\,\text{S/m}$ implies $\sigma_3 \simeq 0.017\,\text{S/m}$. Kosterick et al. (1984) reported $\sigma_3 \simeq 0.012\,\text{S/m}$. Averaging the values reported in Law et al. (1993) suggests $\sigma_3 \simeq 0.018\,\text{S/m}$. Oostendorp et al. (2000) reported $\sigma_3 \simeq$

0.015 S/m. This series of literature seems to imply consistently that $\sigma_3 \simeq 0.015$ S/m and $\sigma_1/\sigma_3 \simeq 10$.

This ratio is lower than the range 20-80 suggested by Nunez and Srinivasan (2005), due partly to a lower estimate of brain conductivity. With this skull conductivity, assuming the brain conductivity $\sigma_1 \simeq 0.33$ S/m (Stok 1987), for example, gives the brain-to-skull ratio $\sigma_1/\sigma_3 \simeq 22$. Early models assumed the brain and scalp conductivity were equal (Rush and Driscoll 1968). If this skull conductivity is compared to the scalp rather than the brain, $\sigma_4/\sigma_3 \simeq 29$.

As discussed in Nunez and Srinivasan (2006), however, the effective conductivity of a single layered skull used in a volume conductor model may be substantially lower than its actual conductivity due to several shunting tissues not included in such models, e.g., extra CSF, middle skull layer, skull blood vessels, and anisotropic white matter. These anatomical features increase the tangential conductivity preferentially, and cause more spatial low-pass filtering of the scalp potentials. This is the same effect the skull has on the potential, so these two anatomical features act in parallel, thereby decreasing the effective skull conductivity. For the purposes of building 3- or 4-sphere head models, therefore, these authors estimate the effective skull conductivity ratio is 20-80, but take $\sigma_1 = \sigma_4$. The simulations here are based upon the scalp-to-skull conductivity ratio $\rho \equiv \sigma_1/\sigma_3$. The non-skull tissue values are taken to be $\sigma_1 = 0.15$ S/m, $\sigma_2 = 1.79$ S/m, $\sigma_4 = 0.44$ S/m. All simulations are repeated for two values of $\sigma_3 = 0.015$ S/m and 1.875×10^{-3} S/m, corresponding to $\rho = 10$ and 80, respectively. These values of ρ span the entire range that can be justified by the above arguments.

2.7. Dipole Source Models

For a dipole current source at location $\vec{a}$ in the brain with dipole moment $\vec{m}$, the scalp potential at surface point $\vec{r}$ may be written

$$\Phi(\vec{r}) = \sum_{n=1}^{\infty} c_n f^{n-1} \vec{m} \cdot \left[\hat{r}\ P_n(\cos\theta) + \hat{t}\ \frac{P_n^1(\cos\theta)}{n} \right] \quad (10)$$

where $f \equiv a/r_4$ is the dipole eccentricity, r_4 is the outer scalp radius, θ is the angle between $\hat{r}$ and $\hat{a}$, $\hat{r}$ is the radial unit vector, $\hat{t}$ is the tangential unit vector, and the c_n are constant coefficients (Salu et al. 1990; Sun 1997). Current conservation ensures that the surface integral of the absolute potential Φ induced by a dipolar current source is zero. This is reflected in (10) by the absence of a constant ($n = 0$) term analogous to c_0 in (1). Thus the potential Φ computed with (10) is referenced to infinity, and denoted with the same symbol.

Two source models were considered, corresponding roughly to two complementary paradigms for electrophysiological analysis: event-related potentials (ERP), and spontaneous or resting EEG. First, single dipoles were placed in the outer brain volume, with random position and orientation. Because EEG is mostly sensitive to cortical activity, the random dipoles were restricted in depth to within 5 cm from r_1. The magnitude of the dipole moments was fixed to 0.1 μA m independent of orientation. This situation is similar to an idealized ERP component with very high SNR. Second, following Nunez et al. (1997), a dense layer of 162 radial dipoles was positioned at constant depth 2 cm measured from r_1. The magnitude of each dipole moment was a random number distributed uniformly on the interval $[-0.1, 0.1]$ μA m. This situation is roughly similar to resting or spontaneous EEG with distributed activity of comparable amplitudes. These dipole moments are in the physiological range, but ultimately are arbitrary, preventing quantitative comparisons between the two source models. Thus detailed numerical comparisons must be limited to the two methods of estimating Φ_{ref}, and the effects of other parameters within each source model.

2.8. Numerical Simulations

Simulations were conducted for each source model as follows. For single dipoles, 10^4 random dipoles generated distributions of $\bar{V}$, c_0, and Φ_{ref}. For dipole sheets, 10^4 random 162-dipole patterns generated corresponding distributions. The second case was faster computationally because, for 162 dipoles with fixed locations, the lead field matrix (for each $N = 19, 65, 129$) was computed only once. These distributions were used to compare the two ways of estimating Φ_{ref}.

For each dipole configuration, the absolute scalp potentials Φ_i were computed using (10). Referenced potentials were computed using $V_i = \Phi_i - \Phi_{\text{ref}}$ with the vertex electrode. The average potential $\bar{V}$ was computed using (5). The spline coefficent c_0 was computed for $m = 3$ and 4. The error measures $E(\bar{V}) \equiv \bar{V} + \Phi_{\text{ref}}$ and $E(c_0) \equiv c_0 + \Phi_{\text{ref}}$ were computed and compared. By definition, the *better* approach is that with its error distribution more tightly peaked around zero. Three measures of these distributions were considered: the mean, standard deviation (STD), and interquartile range (IQR), i.e., the difference between the 75th and 25th percentiles. As the term is used here, the usual IQR was multiplied by 0.7413 to estimate the standard deviation without reference to the tails: for Gaussian distributions, STD = IQR.

3. Results

3.1. Limiting Behavior for Large m

In practice, when computing $g_m(x)$ using (2), the infinite sum is truncated at $n_{\max}$ to approximate the limit $n_{\max} \to \infty$. For $m = 1$, the sum does not converge; the

coefficients decrease as $1/n$ for large n, which integrates to $\ln n$. For $m = 4$, $n_{\max} = 7$ is sufficient to reach numerical precision of 10^{-6} (Perrin et al. 1989). The simulations below used $n_{\max} = 30$ for both $m = 3$ and 4.

Figure 1 shows the function $g_m(x)$ as open circles. For each m, $g_m(x)$ is divided by the constant a_m, defined in (9). The function x is shown by a solid line. Visually speaking, for $m = 3$ and 4 advocated in the literature, the approximation (9) is excellent. Thus the seemingly complicated expression for $g_m(x)$ in (2) may be replaced $a_m x$ in (9), an intuitive function of the angle between the interpolation point and each electrode.

Curiously, although Figure 1 strongly supports the approximation $g_m(x) \simeq a_m x$, a problem arises when attempting to fit the splines. The system of equations (3)–(4) is solved by inversion of an $(N + 1) \times (N + 1)$ matrix. A critical requirement is that the matrix be full rank, otherwise regularization is required and accuracy may be lost. For the 65-electrode array, replacing $g_m(x) \simeq a_m x$ produced a matrix with rank equal not to $(N + 1)$ but only to 5. This prohibits satisfying the basic condition (3), and must be considered invalid. For this reason, it is advisable to use (2) for numerical interpolation. Approximation (9) is used here only to build intuition.

3.2. Performance of Spline-Based Estimate of Φ_{ref}

The errors in estimating Φ_{ref} were evaluated as described in Section 2.8. Figure 2 shows the results for single dipoles, with spline order $m = 3$ and scalp-to-skull conductivity ratio $\rho = 10$. The rows vary electrode numbers $N = 19$ (top), 65 (middle), 129 (bottom). The left column shows the error distributions $E(\bar{V})$; the right column $E(c_0)$. Each distribution is centered about zero; this is expected because the signs of the dipoles are chosen randomly. In the left column, the distributions are dense over their entire range. The distribution for $N = 65$ is single peaked, while those for $N = 19$ and $N = 129$ are

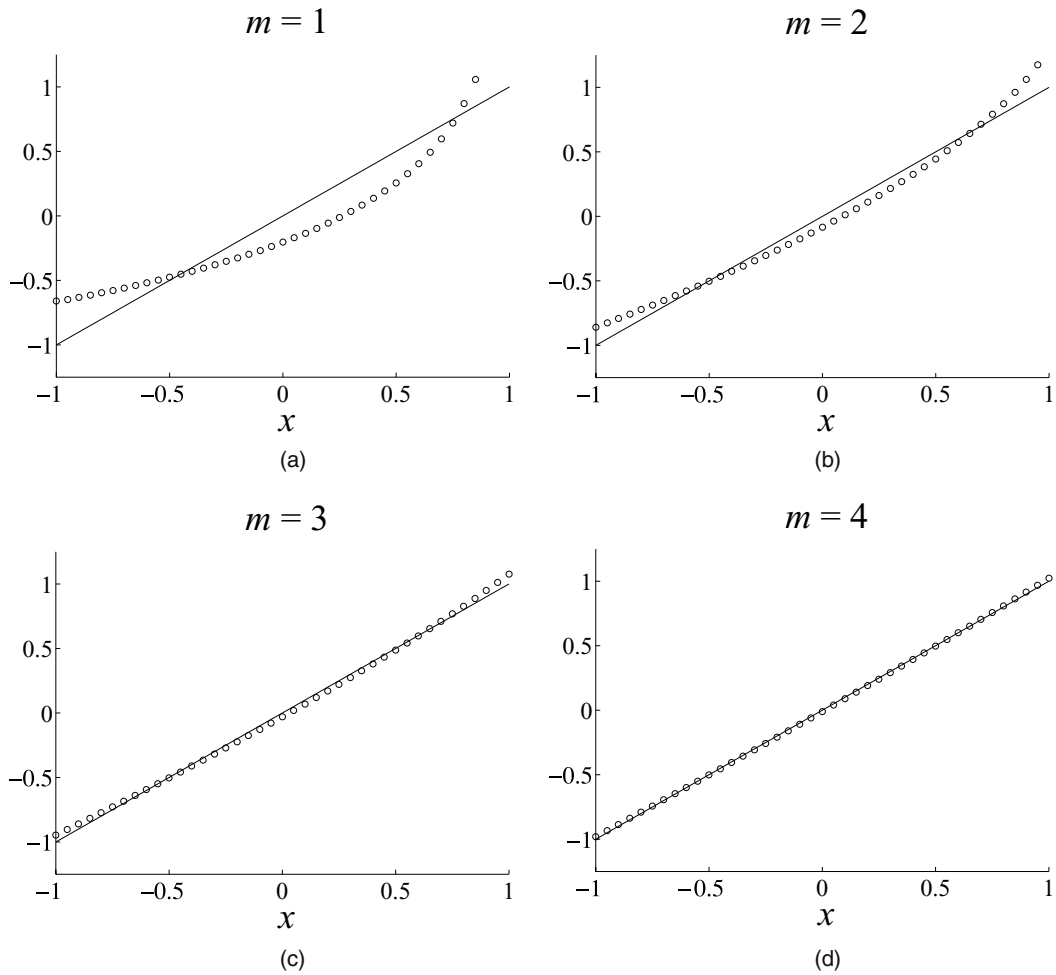

Figure 1. Convergence of the spline function $g_m(x)$ toward $a_m x$ for increasing order m (a) $m = 1$, (b) $m = 2$, (c) $m = 3$, (d) $m = 4$. The sum in (2) was taken to $n_{\max} = 30$. To facilitate comparison, $g_m(x)/a_m$ is shown by *circles*, and the function x is shown by *lines*.

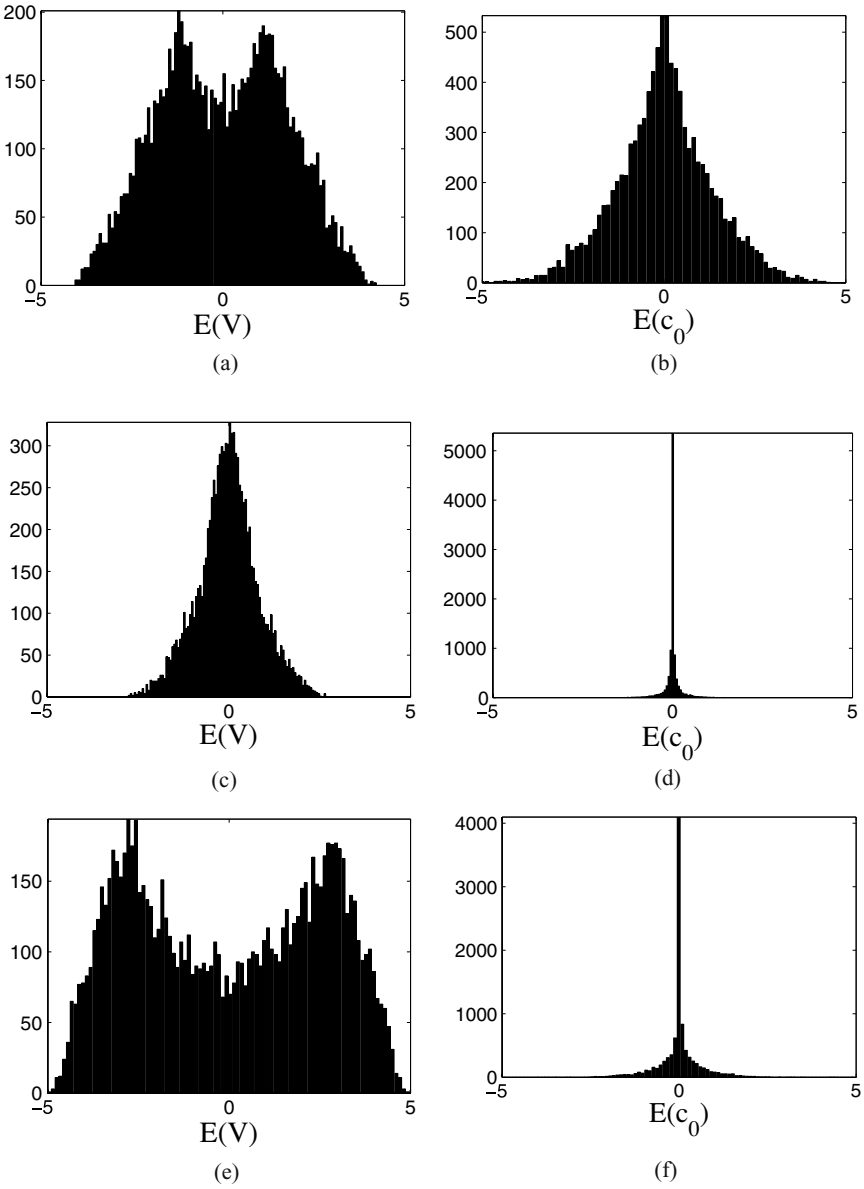

Figure 2. Distributions of errors for the two methods of estimating Φ_{ref}, with $\rho = 10$. Columns span the method: $E(\bar{V})$ (*left*); $E(c_0)$ with spline order $m = 3$ (*right*). Rows span the number of electrodes $N = 19$ (*top*), 65 (*middle*), 129 (*bottom*). Statistics are listed in Table I.

double peaked. In contrast, the error distributions $E(c_0)$ in the right column are sharply peaked with long tails. The maximum and minimum values are comparable for left and right columns, thus $E(c_0)$ more than $E(\bar{V})$ is distributed tightly about zero.

Table I shows the statistics of the error distributions in Figure 2, for single dipoles, $\rho = 10$ and $m = 3$. The means are very close to zero. For $N = 65$ and 129, the STD of $E(c_0)$ is smaller than that of $E(\bar{V})$ by a factor $\simeq 4$. For $N = 19$, the improvement is smaller but also evident. The more striking distinction between the distributions of $E(c_0)$ and $E(\bar{V})$ is quantified by the IQR. For $E(\bar{V})$ the IQR is similar to the STD, especially for $N = 65$ which is near Gaussian. In contrast, for $E(c_0)$ the IQR is smaller than the STD, as expected for a sharply peaked distribution without its tails. For $N = 65$ and 129, the IQR of $E(c_0)$ is smaller than that of $E(\bar{V})$ by a factor $\simeq 70$. For $N = 19$, the improvement is smaller but also evident. Together these results confirm that the splines provide a *better* estimate of Φ_{ref}, especially for $N \geq 65$. Table II shows similar results for $\rho = 10$ and $m = 4$. The errors for $E(\bar{V})$ are nearly identical for $m = 3$ versus $m = 4$. The errors for $E(c_0)$ are slightly different for $m = 3$ and $m = 4$, but these differences are small compared to the differences between $E(\bar{V})$ and $E(c_0)$.

Table I. Single dipoles, $\rho = 10$, $m = 3$

	$E(\bar{V})$			$E(c_0)$		
N	Mean	STD	IQR	Mean	STD	IQR
19	0.00	1.70	1.97	0.00	1.32	1.17
65	0.02	0.84	0.73	0.00	0.23	0.03
129	0.02	2.59	3.60	0.00	0.61	0.15

Table II. Single dipoles, $\rho = 10$, $m = 4$

	$E(\bar{V})$			$E(c_0)$		
N	Mean	STD	IQR	Mean	STD	IQR
19	0.01	1.68	1.94	0.00	1.72	1.30
65	0.00	0.83	0.70	0.00	0.24	0.03
129	0.02	2.60	3.63	0.01	0.75	0.17

Table III. Single dipoles, $\rho = 80$, $m = 3$

	$E(\bar{V})$			$E(c_0)$		
N	Mean	STD	IQR	Mean	STD	IQR
19	0.00	0.81	1.05	0.01	0.34	0.28
65	0.00	0.33	0.32	0.00	0.04	0.00
129	0.01	1.31	1.84	0.00	0.14	0.03

Table IV. Single dipoles, $\rho = 80$, $m = 4$

	$E(\bar{V})$			$E(c_0)$		
N	Mean	STD	IQR	Mean	STD	IQR
19	0.00	0.81	1.03	0.00	0.37	0.31
65	0.00	0.32	0.31	0.00	0.04	0.00
129	0.02	1.31	1.84	0.00	0.14	0.03

Table V. Dipole sheets, $\rho = 10$, $m = 3$

	$E(\bar{V})$			$E(c_0)$		
N	Mean	STD	IQR	Mean	STD	IQR
19	0.06	12.70	12.56	0.04	10.50	10.50
65	0.03	6.37	6.41	0.00	1.12	1.13
129	0.20	19.00	19.08	0.00	4.19	4.25

Table VI. Dipole sheets, $\rho = 10$, $m = 4$

	$E(\bar{V})$			$E(c_0)$		
N	Mean	STD	IQR	Mean	STD	IQR
19	0.06	12.70	12.57	0.15	13.07	13.00
65	0.03	6.37	6.41	0.00	1.06	1.06
129	0.20	18.99	19.08	0.02	4.23	4.29

Tables III and IV show the statistics of the error distributions for single dipoles, with $\rho = 80$. Compared to the results in Tables I and II for $\rho = 10$, the absolute values of the errors are smaller by a factor $\simeq 2$, for the same dipole magnitudes. This difference is mainly attributable to the fact that smaller skull conductivity results in smaller scalp potentials. This echos the point that numerical values of these errors are not trivial to interpret, yet meaningful comparisons may be made between the two methods of estimating Φ_{ref}. The overall behaviors seen in Figure 2 are preserved: the distributions for $N = 19$ and 129 are double peaked, while the distribution for $N = 65$ is nearly Gaussian; this point is elaborated in the Discussion. For $N = 65$ and 129, the STD of $E(c_0)$ is smaller than that of $E(\bar{V})$ by a factor $\simeq 9$, approximately twice that for $\rho = 10$. This finding suggests that, for single dipole sources, the improvement in estimating Φ_{ref} is greater for lower skull conductivity.

Tables V and VI show the statistics of the error distributions for the many-dipole configurations and $\rho = 10$. The results are nearly identical for $m = 3$ and $m = 4$. Visual inspection of the distributions for $E(\bar{V})$ and $E(c_0)$ (not shown), and this numerical finding that IQR $\simeq$ STD, confirm their Gaussian shape. Generally speaking, the absolute values in Tables V and VI are larger than those in Tables I and III, but recall that the choice of dipole magnitudes in each source model were chosen sensibly yet arbitrarily. Thus rigorous numerical comparisons are not possible across source models, but are possible between methods for estimating Φ_{ref}. In nearly all cases, the STD of $E(c_0)$ is smaller than the STD of $E(\bar{V})$. For $N = 65$ and $N = 129$, the improvement is by a factor $\simeq 5$. For $N = 19$, the improvement is small for $m = 3$ and in the wrong direction for $m = 4$.

Tables VII and VIII show the statistics of the error distributions for the many-dipole configurations and $\rho = 80$. The results for $m = 3$ and $m = 4$ are nearly identical. Compared to the results in Tables V and VI for $\rho = 10$, the absolute values of the errors smaller, again attributable partly to the smaller scalp potentials. Comparing the two methods of estimating Φ_{ref}: for $N = 19$ the improvement is by a factor $\simeq 2$; for $N = 65$ the improvement is by a factor $\simeq 11$; and for $N = 129$ the improvement is by a factor $\simeq 10$. These results imply that,

Table VII. Dipole sheets, $\rho = 80$, $m = 3$

	$E(\bar{V})$			$E(c_0)$		
N	Mean	STD	IQR	Mean	STD	IQR
19	0.04	5.94	5.97	0.01	2.70	2.67
65	0.04	2.45	2.43	0.00	0.21	0.21
129	0.05	9.61	9.64	0.00	0.93	0.94

Table VIII. Dipole sheets, $\rho = 80$, $m = 4$

	$E(\bar{V})$			$E(c_0)$		
N	Mean	STD	IQR	Mean	STD	IQR
19	0.03	6.05	5.97	0.03	2.92	2.92
65	0.01	2.45	2.43	0.00	0.18	0.18
129	0.09	9.53	9.53	0.00	0.79	0.80

consistent with the single-dipole source models, the improvement in estimating Φ_{ref} is greater for lower skull conductivity.

4. Discussion

Despite their long and widespread use in scalp EEG, only one paper has advocated the use of spherical splines for estimating the average reference potential (Junghofer et al. 1999). The present paper works out the theoretical basis for this, and shows the results of numerical simulations that elaborate its generality. The theoretical steps involved the isolation of the average reference potential in the standard spline equation (1), and a qualitative assessment of the function $g_m(x)$ for $m \geq 3$. The results suggest that the spline-based estimate is markedly *better* for $N \geq 65$.

At first glance, (1) and (2) are reminiscent of the solution to Poisson's equation for the potential on the surface of a sphere given azimuthal symmetry, e.g., as is generated by radial dipole sources. There are two major differences, however, which may be seen by contrasting (1) and (2) with the dipole solution given in (10). First, the spherical splines involve only the ordinary Legendre polynomials $P_n(x)$, while the dipole solution (10) involves both $P_n(x)$ and the first-order associated Legendre polynomials $P_n^{(1)}(x)$. The two terms in (10) correspond to radial and tangential dipoles, respectively. Second, in (10) the relative weights of the Legendre polynomials of order n are determined by fitting the coefficients c_n to match the boundary conditions of a particular problem. By contrast, in (2) the relative weights are determined by the factor $(2n+1)/(n(n+1))^m$, independent of the coefficients c_j that are fitted to the scalp electrode data. Together these observations emphasize that the spherical splines do not capture the physics of volume conduction in the head. Nevertheless, when applied to EEG, the spherical splines represent the surface potential in a way that is transparent in how to extract the average surface potential, and that is qualitatively compatible with the topography of dipolar fields. This permits the estimation of average referenced potentials with spherical splines.

Two complementary source models were considered, and gave rise to very different error distributions. For scalp EEG, the difference between these two source models is in the sensitivity of a given electrode to near and distant dipoles. A single dipole with high SNR can influence the potential at every electrode. A continuous dipole sheet impacts the electrode array more locally, such that the potential at each electrode is dominated by nearby dipoles averaged over 10-100 cm^2. It is difficult to interpret the absolute values of the errors shown in Tables I−VIII, without knowing the absolute values of the scalp potentials for the same simulations. The dipole moments were chosen to be in the correct physiological range, but the absolute values of the scalp potentials depend upon the scalp-to-skull conductivity ratio and the depth and orientation of each dipole. In the discussion of the numerical results, therefore, clear emphasis is placed on comparing the two methods of estimating Φ_{ref}. The results show improvement factors in the range 5–10, corresponding to several μV in scalp potential. Intuition and the sensible choice of dipole moments and head model parameters suggest that the findings here are meaningful for experimental EEG.

The numerical simulations used three electrode arrays. For $N = 65$ and 129, the improvement in estimating Φ_{ref} with spherical splines was apparent. For $N = 19$, the improvement was smaller, and occasionally in the wrong direction. This result is expected, because $N = 19$ is too few electrodes to adequately sample the scalp surface potential and constrain the spherical splines. Srinivasan et al. (1998) have shown that $N = 65$ is the minimum number of electrodes to adequately sample the scalp potential, and these findings are consistent with theirs. A less intuitive finding is the behavior of the error distributions in Figure 2. For single-dipole sources, the error distributions for $N = 19$ and 129 are double peaked, while for $N = 65$ the error distribution is single peaked. In addition, for every simulation shown in Tables I-VIII, the absolute values of the errors for $N = 65$ are smaller than those for $N = 19$ and $N = 129$. These findings are difficult to interpret, yet several relevant points can be noted. First, the results for $N = 19$ may not be reliable due to poor spatial sampling and spline interpolation, thus the expectation of a smooth trend in absolute errors as a function of N may be too strong. Second, $N = 19$ and 65 arrays were obtained not by sub-sampling the $N = 129$ array, but by taking the measured coordinates from actual electrode arrays on human subjects. Thus not only the sampling density but also the extent of coverage of the three arrays is different, as noted in Section 2.6. Third, although the absolute values of the errors for $N = 65$ are smaller than those for $N = 129$, which may be due to the better ability of the $N = 129$ array to capture sharp peaks and troughs, the improvement factors between $E(\bar{V})$ and $E(c_0)$ are quite similar throughout, suggesting a type of consistency between these results. Despite the difficulty of interpreting this aspect of

the results, the overall conclusions of this paper remain intact.

The concept of the average reference is based on the assumption of a topologically closed surface, which is violated for the scalp. This flaw in the applicability of the average reference concept to scalp EEG is not easily remedied in living subjects, but seems unlikely to cancel the PARE effect. In this sense, the improvement reported here by using the spherical splines to estimate the surface potential is expected to generalize to real experiments. The potentials relative to infinity within the brain and on the inner skull surface are determined almost entirely by the conductivity boundary between the brain (or CSF) and skull (Burger and van Milaan 1943; Hamalainen and Sarvas 1989). The skull forms a closed surface encasing the brain, albeit not spherical or topologically simple. Thus the assumption of a closed surface is probably reasonable for the dura potential. In theory, the potential at the scalp is influenced more by this error at the neck.

This paper has been limited to the spatial aspects of the calculation of the average-referenced potential. Because the errors in estimating the average reference at each time point evolve as a time series, this methodological improvement should generalize to temporal analyses. Many if not most researchers still analyze referenced scalp data. Every temporal measure of EEG computed at measurement electrodes, e.g., event-related potentials, power spectra and coherence, are known to be sensitive to activity at the reference electrode. The scalp average-referenced potential and scalp surface Laplacian are the minimal approaches for removing the reference effect, but the former has fallen into disrepute due to the PARE effect and the availability of the scalp surface Laplacian. Because the scalp surface Laplacian acts as a spatial high-pass filter, however, it should be seen as complementary to the scalp potential, rather than a replacement. Thus the scalp average-referenced potential remains a valuable tool in modern EEG, even in light of the other advances in spatial analysis and source current estimation. Source current estimation will not benefit directly from this development, because forward solutions may always be referenced to match the experimental condition.

Acknowledgments

This work was supported in part by National Institutes of Health grants R43-MH-53768 and R43-NS-38788 while the author was at Electrical Geodesics, Inc. The author thanks Don Tucker and Paul Nunez for helpful discussions.

References

Arfken, G.B. and Weber, H.J. Mathematical Methods for Physicists. Academic Press, 1995.

Baumann, S.B., Wonzy, D.R., Kelly, S.K. and Meno, F.M. The electrical conductivity of human cerebrospinal fluid at body temperature. IEEE Trans. Biomed. Eng., 1997, 44(3): 220–223.

Bertrand, O., Perrin, F. and Pernier, J. A theoretical justification of the average reference in topographic evoked potential studies. Electroenceph. Clin. Neurophysiol., 1985, 62(6): 462–464.

Burger, H.C. and van Milaan, J.B. Measurements of the specific resistance of the human body to direct current. Acta Med. Scand. Fasc. VI, 1943, 114: 584–607.

Desmedt, J.E. and Tomberg, C. Topographic analysis in brain mapping can be compromised by the average reference. Brain Topogr., 1990, 3(1): 35–42.

Duchon, J. Interpolation des fonctions de deux variables suivant le principe de la flexion des plaques minces. RAIRO Anal. Num., 1976, 10: 5–12.

Fletcher, E.M., Kussmaul, C.L. and Mangun, G.R. Estimation of interpolation errors in scalp topographic mapping. Electroenceph. Clin. Neurophysiol., 1996, 98: 422–434.

Gencer, N.G., Williamson, S.J., Gueziec, A. and Hummel, R. Optimal reference electrode selection for electric source imaging. Electroenceph. Clin. Neurophysiol., 1996, 99(2): 163–173.

Geselowitz, D.B. The zero of potential. IEEE Eng. Med. Biol. Mag., 1998, 17(1): 128–132.

Hamalainen, M.S. and Sarvas, J. Realistic conductor geometry model of the human head for interpretation of neuromagnetic data. IEEE Trans. Biomed. Eng., 1989, 36: 165–171.

Hjorth, B. An on-line transformation of EEG scalp potentials into orthogonal source derivations. Electroenceph. Clin. Neurophysiol., 1975, 39: 526–530.

Junghofer, M., Elbert, T., Tucker, D.M. and Braun, C. The polar average reference effect: A bias in estimating the head surface integral in EEG recording. Clin. Neurophysiol., 1999, 110(6): 1149–1155.

Law, S.K., Nunez, P.L. and Wijesinghe, R.S. High-resolution EEG using spline generated surface Laplacians on spherical and ellipsoidal surfaces. IEEE Trans. Biomed. Eng., 1993, 40(2): 145–153.

Lehmann, D., Ozaki, H. and Pal, I. Averaging of spectral power and phase via vector diagram best fits without reference electrode or reference channel. Electroencephalogr. Clin. Neurophysiol., 1986, 64(4): 350–363.

Nunez, P.L. Electric fields of the brain: The neurophysics of EEG. New York, Oxford University Press, 1981.

Nunez, P.L. and Srinivasan, R. Electric fields of the brain: The neurophysics of EEG, 2nd edition. New York, Oxford University Press, 2006.

Nunez, P.L., Srinivasan, R., Westdorp, A.F., Wijesinghe, R.S., Tucker, D.M., Silberstein, R.B. and Cadusch, P.J. EEG coherency. I: Statistics, reference electrode, volume conduction, Laplacians, cortical imaging, and interpretation at multiple scales. Electroencephalogr. Clin. Neurophysiol., 1997, 103(5): 499–515.

Orekhova, E.V., Wallin, B.G. and Hedstrom, A. Modification of the average reference montage: Dynamic average reference. J. Clin. Neurophysiol., 2002, 19(3): 209–218.

Perrin, F., Pernier, J., Bertrand, O., Giard, M.H. and Echallier, J.F. Mapping of scalp potentials by surface spline interpolation. Electroenceph. Clin. Neurophysiol., 1987, 66: 75–81.

Perrin, F., Pernier, J., Bertrand, O. and Echallier, J.F. Spherical splines for scalp potential and current density mapping. Electroenceph. Clin. Neurophysiol., 1989, 72: 184–187.

Perrin, F., Pernier, J., Bertrand, O. and Echallier, J.F. Corrigenda: EEG 02274. Electroenceph. Clin. Neurophysiol., 1990, 76: 565.

Press, W.H., Tuekolsky, S.A., Vetterling, W.T. and Flannery, B.P. Numerical recipes in C. Cambridge University Press, 1992.

Rush, S. and Blanchard, R.R. Skull physical and electrical characteristics relevant to the distribution from electrodes on the scalp. Proceedings of the 19th ACEMB, 1966.

Rush, S. and Driscoll, D.A. Current distribution in the brain from surface electrodes. Anesthesia analgesia, 1968, 47(6): 717–723.

Salu, Y., Cohen, L.G., Rose, D., Sato, S., Kufta, C. and Hallett, M. An improved method for localizing electric brain dipoles. IEEE Trans. Biomed. Eng., 1990, 37: 699–705.

Soong, A.C.K., Lind, J.C., Shaw, G.R. and Koles, Z.J. Systematic comparisons of interpolation techniques in topographic brain mapping. Electroenceph. Clin. Neurophysiol., 1993, 87: 185–195.

Soufflet, L., Toussaint, M., Luthringer, R., Gresser, J., Minot, R. and Macher, J.P. A statistical evaluation of the main interpolation methods applied to 3-dimensional EEG mapping. Electroenceph. Clin. Neurophys., 1991, 79: 393–402.

Srinivasan, R., Tucker, D.M. and Murias, M. Estimating the spatial Nyquist of the human EEG. Behav. Res. Methods, Instrum. Comput., 1998, 30: 8–19.

Stok, C.J. The influence of model parameters on EEG/MEG single dipole source estimation. IEEE Trans. Biomed. Eng., 1987, 34(4): 289–296.

Sun, M. An efficient algorithm for computing multishell spherical volume conductor models in EEG dipole source localization. IEEE Trans. Biomed. Eng., 1997, 44(12): 1243–1252.

Tomberg, C., Neol, P., POzaki, I. and Desmedt, J.E. Inadequacy of the average reference for the topographic mapping of focal enhancements of brain potentials. Electroenceph. Clin. Neurophys., 1990, 77(4): 259–265.

Wahba, G. and Wendelberger, J. Some new mathematical methods for variational objective analysis using splines and cross validation. Mon. Weather Rev., 1980, 108: 1122–1143.

Wahba, G. Spline interpolation and smoothing on the sphere. SIAM J. Sci. Stat. Comput., 1981, 2(1): 5–16.

Wahba, G. Erratum: Spline interpolation and smoothing on the sphere. SIAM J. Sci. Stat. Comput. 1982, 3(3): 385-386.

Yao, D. A. method to standardize a reference of scalp EEG recordings to a point at infinity. Physiol. Meas., 2001, 22(4): 693–711.